Assessment of Unstructured Grids for Detached-Eddy Simulation of High Reynolds Number Separated Flows

Scott A. Morton and James R. Forsythe
Dept. of Aeronautics
USAF Academy, CO 80840

Kyle D. Squires
Dept. of Mech. and Aerospace Engineering
Arizona State University
Tempe, AZ 85287

Kenneth E. Wurtzler
Cobalt Solutions, LLC
Miamisburg, OH 45459

Abstract

An assessment of unstructured grids for use in Detached-Eddy Simulation (and more generally in Large-Eddy Simulation) of massively separated flows is presented. The role of the grid, its generation and refinement, are considered via calculation of three high-Reynolds number turbulent flows of aerodynamic interest: the massively separated flow over a forebody in crossflow, the flow over a delta wing at 27° angle of attack, and the flow around an F-15E at 65° angle of attack. Unstructured grids are generated using Gridgen and VGRIDns and are evaluated against guidelines proposed by Spalart[4], which outline the unique requirements of Detached-Eddy Simulation grids. For each geometry, the grids are characterized by a "viscous region" comprised of prism layers, with the "focus region" formed from nearly-isotropic tetrahedra. Predictions of the flow around the forebody show qualitatively similar wake structures, and very close pressure distributions obtained using structured and unstructured grids. Extensive grid refinement is performed for the delta wing and the F-15E, with systematic refinement accomplished via straightforward changes to a grid control parameter. Baseline grids are refined and coarsened by $\sqrt{2}$ in all three coordinate directions, and the time step is varied by the same scale factor. A tangibly wider range of turbulent length scales is captured on the finer grids, with the coarser grids also showing a reasonable scale range. The capability of unstructured grids to meet Spalart's[4] guidelines and the ability to rapidly refine these grids to reduce numerical errors is demonstrated.

Introduction

An important class of turbulent flows of aerodynamic interest are those characterized by massive separation, e.g., the flow around an aircraft at high angle of attack. Numerical simulation is an important tool for analysis, though traditional models used in the solution of the Reynolds-averaged Navier-Stokes (RANS) equations appear unable, by their very design, to accurately account for the time-dependent and three-dimensional motions governing flows with massive separation. Large Eddy Simulation (LES) is able to resolve these unsteady three-dimensional motions, but is cost prohibitive for high Reynolds number wall-bounded flows due to the need to resolve the small scale motions in the boundary layer.

To circumvent the drawbacks of current approaches Spalart *et al.*[1] proposed a hybrid technique, Detached-Eddy Simulation (DES), which takes advantage of the often adequate performance of RANS turbulence models in the "thin", typically attached regions of the flow, not far from the training ground where the models are calibrated. In the separated regions of the flow the technique becomes a Large Eddy Simulation (LES), directly resolving the time-dependent and unsteady features that dominate regions of massive separation. DES has now been applied to a range of challenging test cases, typically yielding more accurate predictions than can be obtained with RANS (e.g., see Strelets[2], Squires *et al.*[3]).

A powerful feature of DES is that it directly resolves turbulent eddies with increasing fidelity as the grid is refined. Note that in RANS it is the mean flow that is computed, the role of grid refinement is to ensure convergence of the numerical solution and to minimize (or eliminate) the influence of the grid. In the fine-grid limit, the accuracy of RANS predictions are controlled by the turbulence model. In LES and DES, on the other hand, the role of grid refinement is resolution of additional physical features, i.e., a wider range of turbulent eddies are represented as grid spacings are decreased. Correspondingly, the contribution of the turbulence model to the solution decreases as the grid is refined. The fine-grid limit of DES (and LES) is a solution free of turbulence modeling errors, i.e., a Direct Numerical Simulation (DNS).

Convergence towards DNS is a well-known feature of LES, though an approach to systematic grid refinement in complex configurations is a challenging task. LES studies on structured grids, for example, have seldom considered simultaneous refinement in all three coordinate directions. This complicates interpretation since, away from solid surfaces, the smallest resolved scale will be determined by the coarsest of the three grid spacings and there is little advantage to finer spacing in a given direction[4].

The objective of the present contribution is an examination of the role of the grid, including its generation and refinement, on DES predictions of massively separated flows. Calculations of complex configurations are performed on unstructured grids and one of the primary aims of this study is to develop a systematic approach to grid refinement in eddy-resolving calculations. In a related effort, Spalart[4] has described the process of grid design and assessment for DES, defining important regions in the solution and offering guidelines for grid densities within each region. The "Young-Person's Guide to Detached-Eddy Simulation Grids,"[4] (YPG) forms a basis for interpretation of many of the results presented below, the focus in this contribution being on unstructured grids.

One of the traditional motivations for unstructured grids has been the ability to rapidly create grids around complex geometries. There are other positive attributes of unstructured grids that are relevant to DES. It is possible, for example, to concentrate points in regions of interest – the "focus region" introduced in the YPG – and to rapidly coarsen the grid away from these areas. Another advantage exploited in the present investigations are isotropic grid cells in the "LES region" of a DES. The YPG pointed out the desirability of isotropic grid cells (cubic for a structured grid) in the focus region in which unsteady, time-dependent features are resolved. As discussed in greater detail in the following section, unstructured grids are good candidates for use in DES because near isotropy of the grid cells in the LES region is assured by most grid generation packages.

In the following section, the DES technique is outlined, along with a summary of the numerical approach used for solution of the discretized system, and details on the grid generation procedures. Calculations of three geometries are presented: the flow around a model of an aircraft forebody in a crossflow, the flow over a delta wing at 27° angle of attack, and flow around a full aircraft (F-15E at 65° angle of attack). The flow around the forebody cross-section and delta wing each contain elements relevant to the F-15E; each flow field is distinctly different, challenging the turbulence model and, perhaps more importantly, the grid. Features of the solution are assessed with respect to the grid, e.g., the influence of grid refinement and some comparison to predictions of the same flow on structured grids.

Computational Approach

Detached-Eddy Simulation

The DES formulation in this study is based on a modification to the Spalart-Allmaras RANS model[6] such that the model reduces to its RANS formulation near solid surfaces and to a subgrid model away from the wall[7].

The basis is to attempt to take advantage of the usually adequate performance of RANS models in the thin shear layers where these models are calibrated and the power of LES for resolution of geometry-dependent and three-dimensional eddies. The DES formulation is obtained by replacing in the S-A model the distance to the nearest wall, d, by $\widetilde{d}$, where $\widetilde{d}$ is defined as,

$$\widetilde{d} \equiv \min(d, C_{DES}\Delta)\,. \tag{1}$$

In "natural" applications of DES, the wall-parallel grid spacings (e.g., streamwise and spanwise) are at least on the order of the boundary layer thickness and the S-A RANS model is retained throughout the boundary layer, i.e., $\widetilde{d} = d$. Consequently, prediction of boundary layer separation is determined in the "RANS mode" of DES. Away from solid boundaries when the production and destruction terms of the model are balanced, the length scale $\widetilde{d} = C_{DES}\Delta$ in the LES region yields a Smagorinsky-like eddy viscosity, $\widetilde{\nu} \propto S\Delta^2$. Analogous to classical LES, the role of Δ is to allow the energy cascade down to the grid size; roughly, it makes the pseudo-Kolmogorov length scale, based on the eddy viscosity, proportional to the grid spacing. The additional model constant $C_{DES} = 0.65$ was set in homogeneous turbulence[8] and was used without modification in all of the calculations described below.

Flow solver

The computations were performed using the commercial solver Cobalt. Cobalt is an unstructured finite-volume method developed for solution of the compressible Navier-Stokes equations; details on the approach are described in Strang *et al.*[5]. The method is a cell-centered finite volume approach applicable to arbitrary cell topologies (e.g, hexahedra, prisms, tetrahedra). The spatial operator uses an exact Reimann Solver, least squares gradient calculations using QR factorization to provide second order accuracy in space, and TVD flux limiters to limit extremes at cell faces. A point implicit method using analytic first-order inviscid and viscous Jacobians is used for advancement of the discretized system. For time-accurate computations, a Newton sub-iteration scheme is employed with the time-integration scheme up to second-order accurate in time. For all calculations, second-order accuracy in space and time were used, with a minimum of two Newton subiterations.

Grids

The unstructured grids on the delta wing and the F-15E were created using VGRIDns[9] – a grid generator developed at the NASA Langley Research Center. The surface definition was first established using GridTool (http://geolab.larc.nasa.gov/GridTool). The viscous region[4] was then grown by VGRIDns using the advancing layers method. This allowed specification of an initial wall-normal coordinate for the first cell nearest a solid surface and a geometric progression for the cells above. Although VGRIDns grows a tetrahedral viscous grid, the Cobalt utility *blacksmith* was used to recombine the tetrahedra into prisms. This provides a more orthogonal grid while reducing the cell count.

VGRIDns was then used to fill the remaining volume with near isotropic tetrahedra, using the advancing front method. The isotropic tetrahedra are desired in DES applications since such cell-types ensure the lowest value of Δ for a given cell volume, lowering the eddy viscosity and allowing more fluctuations to be resolved on the grid. Also, since the orientation of turbulent structures are not necessarily known *a priori*, isotropic cells are a logical approach to resolving turbulent length scales. The YPG defines the average cell size in the focus region as Δ_0. The number of cells does not grow quite as rapidly as $1/\Delta_0^3$, because the wall-normal resolution in the first layers is not changed, unless indicated otherwise.

To define grid spacing, VGRIDns uses "background sources" which can be placed independently of the geometry. The cell spacing at any location in the grid is a function of the distance to each source, source strengths, and source spacing. The baseline grids used very small sources on the body and in the focus region, and large sources in the farfield. VGRIDns allows the spacing for all sources to be multiplied by a user-defined input (*ifact*), which is in general equal to unity. This enabled rapid grid refinement or coarsening by simply changing the value of *ifact*, and regenerating the grid.

Results

Flow around a forebody cross-section

Computations of the separated flow around a forebody cross-section provide insight into aspects of the modeling approach adopted in this work and the opportunity to assess DES predictions of a simplified configuration using both structured and unstructured grids. The flow considered is that around a rounded-corner square. The corner radius is 1/4 of the width/height ("diameter", D) of the forebody, similar to the cross-sections of the X-29 and T-38. Numerical predictions are compared to the experimental measurements from Polhamus[10]. They measured forces on a variety of forebody cross-sections over a range of Reynolds numbers and angles of attack.

Unstructured grids for the forebody were generated using Gridgen[12], with prisms in the boundary layer and near-isotropic tetrahedra away from solid surfaces. The prism layer comprises the RANS region of the calculation, with wall-normal spacing appropriate for the S-A model (first surface-normal grid point approximately one viscous unit from solid surfaces, geometric stretching using a factor of 1.2 close to the wall), and wall-parallel spacings on the order of the boundary layer thickness. The ability to exert greater control on cell distribution compared to structured grids permitted generation of an unstructured grid having 2.5×10^6 cells (of a total cell count of 3.55×10^6 cells) within two diameters of the model surface. Comparison to predictions obtained on a structured grid comprised of approximately 4.5×10^6 cells are also shown below. The spanwise dimension was three diameters for both grid-types.

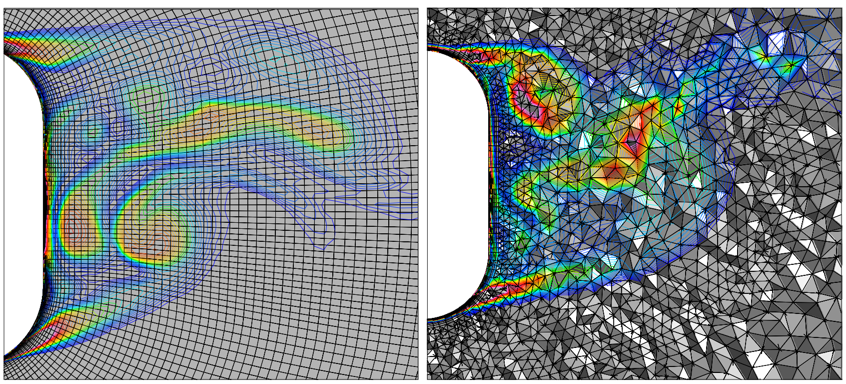

Figure 1. Contours of the instantaneous vorticity magnitude in the forebody near-wake.

Vorticity visualizations in one plane in the near wake from calculations on the structured and unstructured grids are shown in Figure 1. The Reynolds number based on the forebody diameter and freestream velocity is 8×10^5, the angle of attack is $10°$. Experimental measurements indicate separation of turbulent boundary layers near the upper and lower corners at the back of the forebody. The visualizations from both grid-types show qualitatively similar features with a range of eddies resolved in the wake region. As shown by the figure, the grid density in the wake for the two grids is roughly comparable, consistent with about the same scale ranges captured on the two grids. For both grid-types, points were concentrated in the focus region behind the forebody. The clustering is more efficient using the unstructured grid, i.e., Figure 1 shows approximately the same resolution in the wake, though the unstructured grid has, overall, a lower cell count than the structured grid. For the single-block structured grid employed in the forebody computation, there is a higher density of points far from the body where the resolution offered by the structured grid is not required. A Chimera strategy could reduce the grid count for the structured grid, though such a strategy was not attempted in this effort.

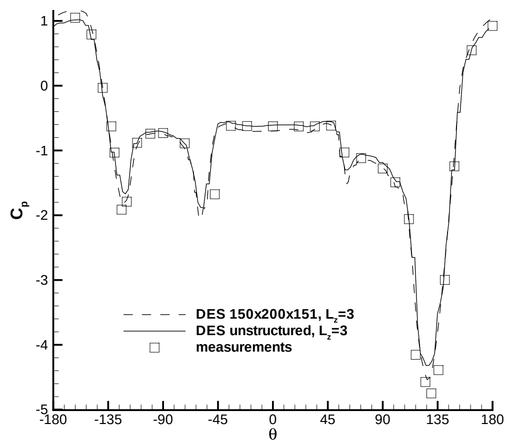

Figure 2. Pressure coefficient distribution around the forebody. Symbols are measurements from Polhamus[10].

Pressure coefficients around the body for the structured and unstructured grids are shown in Figure 2. The distributions shown in the figure were obtained by time averaging the DES predictions for roughly 100 non-dimensional time units. The angle θ is measured counter-clockwise from the aft-symmetry point of the forebody. The maximum C_p occurs about $15-20^{\circ}$ below the fore-symmetry point ($\theta \approx -160^{\circ}$ as shown in Figure 2). Consistent with the flow visualizations above, showing similar structures, Figure 2 shows that the statistical features are also similar for the unstructured and structured grid. The over-prediction of the stagnation C_p from the structured-grid prediction arises from the constraining effect of the computational domain, with influence of the outer boundaries resulting in the over-prediction. The computational domain in the calculation on the unstructured grid was larger and the figure shows a reduction in the stagnation pressure with overall slightly improved agreement against measurements. Normal and axial forces were within 10% of the experimental values for DES, while LES and two-dimensional unsteady RANS predictions were substantially inaccurate, with differences of over 80% in either the axial or normal forces[11].

Delta Wing at $27°$ *Angle of Attack*

The second application of the YPG grid strategy is a slender, sharp-edged, $70°$ delta wing at $27°$ angle of attack. The simulation was run at 24 m/s, a Mach number of 0.069, and other freestream conditions consistent with a Reynolds number of 1.56×10^6. No attempt was made to model transition from laminar to turbulent flow on the delta wing. Typical unsteady simulations were run for 10,000 time steps with an iteration plus either two or three subiterations per time step.

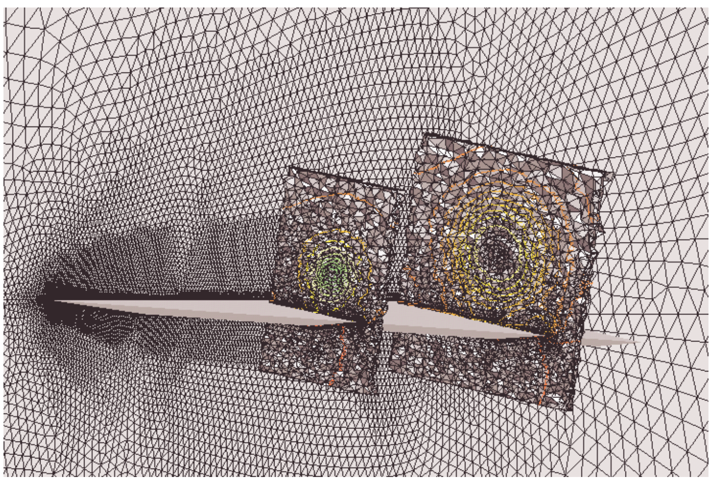

Figure 3. 70 degree delta wing grid with cross planes of vorticity.

A baseline grid consisting of 2.47×10^6 cells was used to determine a time step that is in good balance with the grid (Figure 3). The average wall normal spacing in viscous wall units was 0.85 and there were 13 layers of prisms with an initial geometric growth factor of 1.2. Time step, nondimensionalized by the root chord and the freestream velocity, was varied from 0.00125 to 0.04. Figure 3 depicts the grid structure and also shows contours of vorticity in the cross plane. It is important to notice the refinement of the grid in the focus region of this application, the vortex core.

Time accuracy was assessed by computing solutions for a variety of nondimensional time steps and number of subiterations for the baseline grid above and presented in Morton *et al.*[13]. Using frequency domain analysis from MATLAB, it was determined that the dominant frequency was captured for a nondimensional time step of 0.0025 and three subiterations. This time step is consistent with the YPG guidelines for the given focus region. Assuming a local CFL of 1 and a maximum velocity in the focus region equal to twice the freestream velocity, the YPG guidance for time step is approximately equal to 0.0025. The following grid sensitivity analysis uses this time step as a baseline and then scales it based on the grid density in the focus region for additional grids.

Next, an assessment of vortex breakdown behavior with grid density was made. A grid similar to the baseline grid, termed the medium grid, was developed that had 2.671×10^6 cells. The focus region had cell sizes of 0.0065 chords and the same wall normal spacing as the baseline grid. Coarser and finer grids were then generated by applying an *ifact* of $\sqrt{2}$ and $1/\sqrt{2}$. Table 1 summarizes the details of the three grids.

	Cells	Δ_0 (chords)	Δt^*
coarse	1.188×10^6	0.0046	0.00357
medium	2.671×10^6	0.0065	0.0025
fine	6.565×10^6	0.0035	0.0018

Table 1. Delta wing grid details.

Figure 4 depicts the flowfield solutions at the $10{,}000^{th}$ time step for the coarse, medium, and fine grids. All three grid systems capture vortex breakdown, as well as the post-breakdown helical structures. The medium grid begins to show evidence of additional vortex structures winding around the primary vortex up to the breakdown position. The windings are even more evident in the fine grid. The breakdown position is also varying with grid density. The position moves slightly aft as grid is improved, thus becoming more in line with the experiment[14].

To determine the vortex core behavior with grid refinement, turbulent kinetic energy (TKE) along the core was analyzed and is depicted on the left side of Figure 5. The maximum TKE in the core, nondimensionalized by the freestream velocity squared, increased from 0.17 for the coarse grid to 0.22 for the medium grid and 0.45 for the fine grid. The maximum TKE in the core was found in the experiments to be 0.5[14]. Although the peak value of TKE has doubled between the medium and fine grids, the position of breakdown, as measured by the rapid rise in TKE, is nearly identical. Also, the value of TKE at the aft end of the delta wing is similar.

The right side of Figure 5 for the delta wing shows DES is able to resolve more unsteady flow features as the grid is refined. This Figure shows MAT-

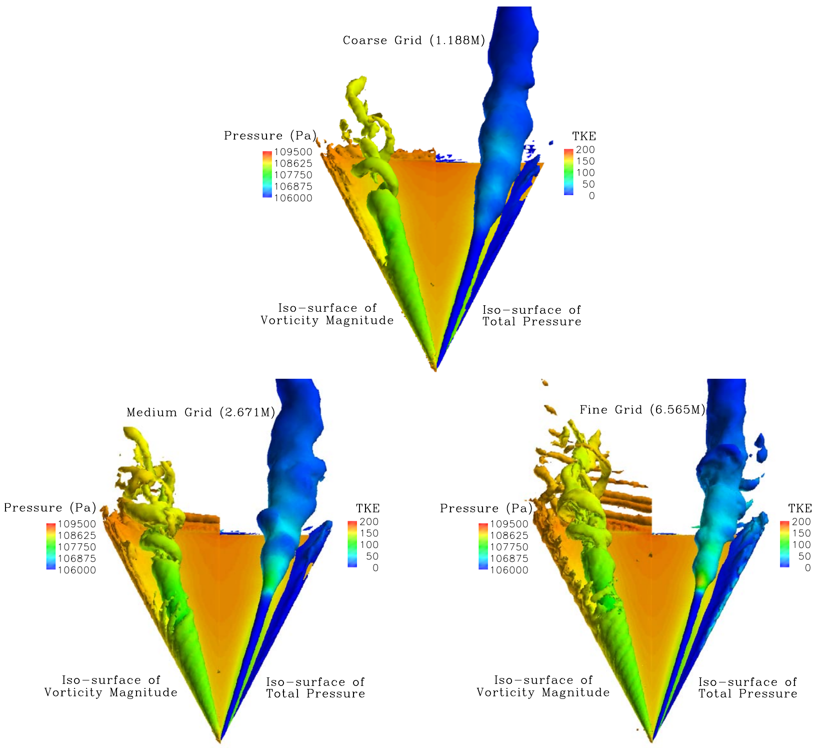

Figure 4. Flowfield solutions for three grids containing iso-surfaces of vorticity magnitude and total pressure.

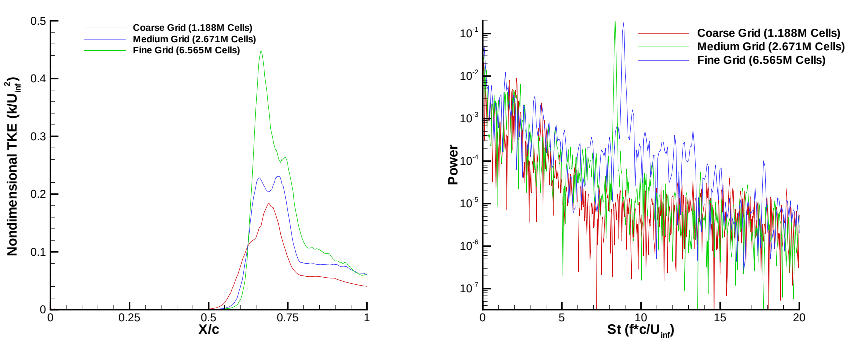

Figure 5. Turbulent kinetic energy along the core and power spectral density plots of the normal force.

LAB power spectral density (PSD) plots for the three grids. As one can see, the frequency content for the fine grid is increased by an order of magnitude in the range from 8 to 15. This additional content is a direct result of resolving the finer scale eddies with improved resolution in the focus region. The ability to capture these high frequency phenomena with grid refinement is crucial for multi-disciplinary problems such as aeroelasticity. It should also be noted that the dominant frequency is in good agreement between the medium and fine grids.

F-15E at 65° *Angle of Attack*

In order to test the capability of DES to predict aerodynamic coefficients at high angles-of-attack, computations were performed of the flow over a clean F-15E with no control deflections at $\alpha = 65^\circ$, Mach $= 0.3$, and standard day 30,000 feet conditions. This resulted in a chord-based Reynolds number of 13.6×10^6. Comparisons were made to Boeing's Stability and Control Database[16]. DES predictions were obtained with a minimum non-dimensional timestep of 0.01 (made dimensionless using the mean chord and freestream velocity). At high Reynolds number the tight clustering in the boundary layer led to a maximum CFL of over 500,000. The CFL outside the boundary layer was on the order of unity, as recommended in the YPG. Since the boundary layer is treated by RANS it is not expected to be a source of instabilities, and therefore large CFL numbers are not problematic if the flow solver can stably integrate the discretized system.

A baseline grid for half of the F-15E was created using VGRIDns[9] and is shown in Figure 6. The original grid consisted of 7.9×10^6 tetrahedral cells. Using the Cobalt grid utility *blacksmith*, nine layers in the boundary layer were combined into prisms, reducing the total number of cells to 5.9×10^6 for the baseline grid. The dimensions of the outer boundaries were 73 chord lengths in the pitch plane, and 18 chord lengths in the yaw plane, as seen in the left frame of Figure 6. A sample region of the viscous layer is shown in the upper right of Figure 6, with the last prism layer barely visible. The distance from solid surfaces to the first cell center normal to the wall was constant, resulting in an average distance in wall units of 0.7. Cell growth in the wall-normal direction was specified using a geometric stretching factor of 1.3. The lower right frame of Figure 6 shows the dense packing of cells close to the aircraft. There were approximately 160,000 faces on the surface of the aircraft with only a few hundred cells on the outer boundary, illustrating the capability of unstructured grids to satisfy one of the aspects outlined in reference [4] – a concentration of points in the focus region.

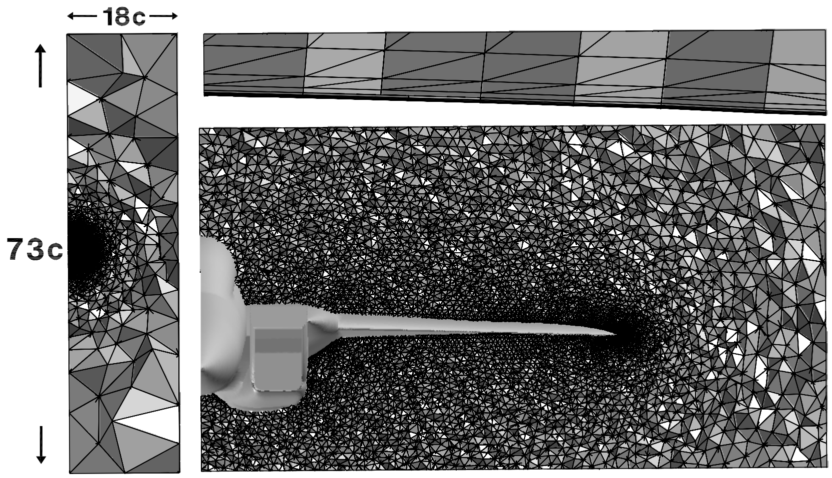

Figure 6. Baseline computational grid for the F-15E. Left: cutting plane of entire computational domain, upper right: viscous layer above the wing, right: cutting plane 680 inches behind aircraft reference point

Sensitivity to the grid was examined via computations using two additional grids (see Figure 7), one coarser and the other finer than the baseline grid. Generation of the baseline grid required one week using VGRIDns[9]. Each additional grid was created in one day. The bulk of the time required to generate the additional grids from the baseline grid was the computation time required to grow the new grid using the modified spacing. The coarse grid was created by modifying the baseline grid sources. For the coarse grid the same distribution of sources were used as in the baseline grid, but with the source sizes increased by $\sqrt{2}$. This was achieved by modifying *ifact* as previously described. This led to approximately 90,000 faces on the surface of the aircraft and a total of 2.85×10^6 cells (mixed tetrahedra and prisms). The viscous spacing and growth rate were left unchanged compared to the baseline grid. For the fine grid, the source sizes on the aircraft surface was divided by $\sqrt{2}$ (again, using *ifact*) with the outer boundary spacing left unchanged (by manually increasing these source strengths by $\sqrt{2}$ prior to changing *ifact*). This resulted in approximately 220,000 faces on the aircraft surface and 10×10^6 cells (mixed tetrahedra and prisms). The geometric cell growth rate in the wall-normal direction was reduced from 1.30 to 1.25. The average wall normal spacing in viscous wall units was less than one for all grids.

Both RANS and DES calculations were performed on all three grids. Fig-

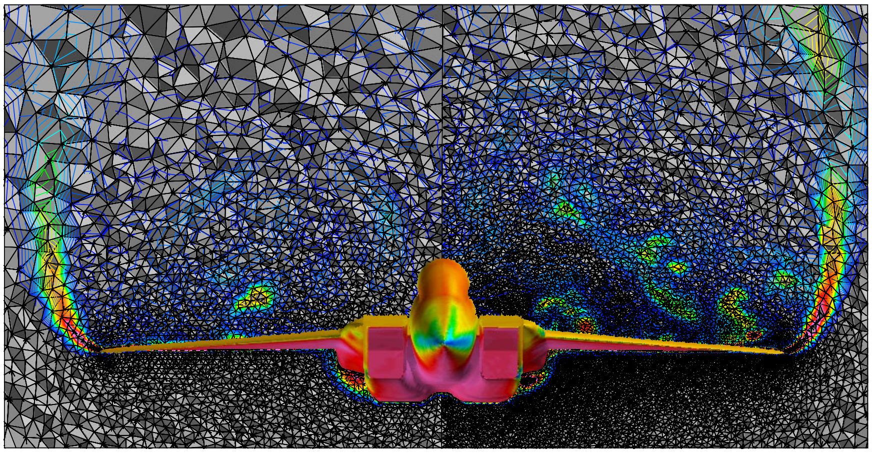

Figure 7. Comparison of coarse (2.85×10^6) and fine (10.0×10^6) grids. Instantaneous vorticity contours at 680 inches behind the aircraft reference point.

ure 7 shows contours of vorticity overlaid on the grid. The LES character of DES yields a wider range of scales as grid spacings are reduced, an effect visible in the contours. Note that even the coarse grid resolves at least some unsteady flow features, e.g., with a few small structures visible above the wing.

		C_L	C_D	C_M
	database	0.781	1.744	-0.466
DES	coarse	0.747	1.677	-0.431
	medium	0.736	1.616	-0.495
	fine	0.759	1.648	-0.457
S-A	coarse	0.855	1.879	-0.504
	medium	0.852	1.867	-0.523
	fine	0.860	1.880	-0.507

Table 2. Averaged lift, drag, and moment coefficients.

The time-averaged drag, lift, and moment coefficients along with their percentage errors compared to the Boeing database are summarized in Table 2. The S-A predictions are relatively accurate in the mean, an interesting finding given the model is applied to prediction of a flow far from its calibration range. Note that for the current configuration at high angle of attack the prediction of flow separation is less challenging than at lower α due to the fixed separation line at the leading edge of the wing. This feature decreases modeling error and assists in obtaining more accurate predictions. The S-A results show little sensitivity to the grid refinement except for the pitching moment. The DES results show more variation with the grid, some of this variation may be an indicator of the need to time-average over a longer period. In general, Table 2 shows that the DES predictions are more accurate with respect to the flight-test data, with percentage errors smaller by as much as a factor of two in the drag coefficient predictions, for example. As the grid is refined, modeling errors are reduced as more flow features are resolved.

Detailed analysis of the grid refinement study in [15] showed that the wing was well resolved with negligible differences in pressure between the three grids. The larger variations in pitching moment were due to the variations in pressure on the nose and horizontal stabilizer as the grid was refined. This analysis will aid in designing a grid that concentrates points in regions of the flow that appear not yet fully grid-converged, in turn reducing modeling errors and improving the overall accuracy of the calculations. Keep in mind, that since DES resolves more flow features as the grid is refined, a strictly grid-converged solution is only reached in the DNS limit. This also applies to LES. Consequently, for an engineering application, grid convergence for DES must be defined in terms of the parameters of interest – time averaged surface pressures in the context of the F-15E, but for other applications it will include unsteady pressures, noise, and so on.

Conclusions

Unstructured grids were used to obtain DES predictions of the flow around a model of an aircraft forebody in a crossflow, the flow over a delta wing at 27° angle of attack, and flow around a full aircraft (F-15E at 65° angle of attack).

Solutions of the flow around the forebody demonstrated the potential of unstructured grids for application in DES, even with an upwind-biased scheme. Predictions obtained using the unstructured grid were similar, both in the qualitative features shown by flow visualizations and in quantitative measures of the pressure distribution, to results obtained on a structured grid. As also shown, DES predictions of the pressure distribution for both grid-types agree well with measurements, substantially better than can be obtained in LES with a poorly resolved wall layer or using RANS. The delta wing predictions also increased confidence in unstructured-grid DES with turbulent kinetic energy in the core of the vortex in close agreement to experiments on the fine grid. For both the forebody and delta wing, the instabilities leading to chaotic and three-dimensional wake structures are quite strong. Calculations of flows with weaker instabilities such as a channel flow may reveal a need for further improvements in DES.

The approach outlined by the YPG for generating DES grids was used as a guideline for the current study. There were no real problems encountered in meeting these guidelines, increasing confidence that the approach outlined in reference [4] is practical. The viscous region was filled with prisms with geometric growth rates less than 1.3, and the first cell center within one viscous unit of the wall. Cells were concentrated in the focus region without needless propagation to the farfield as would potentially be encountered in non-Chimera structured grids. The most fortunate feature in the assessment of the unstructured grids against the criteria in reference [4] was the natural near isotropic cells outside the viscous region. This offers a potential advantage of unstructured grids over structured grids, where obtaining isotropic cells in the focus region will probably be at least slightly more difficult on complex geometries. This advantage could be offset to a greater or lesser extent since there has been far more success constructing higher order methods on structured grids.

Finally, the ability to do a systematic grid refinement on complex geometries with unstructured grids was demonstrated. By globally altering the source sizes within VGRIDns, coarse and refined grids were created on both the delta wing and the F-15E in one to two days. The grid refinement was uniform in all three coordinate directions and uniform throughout the domain (unless otherwise requested). Refining simultaneously in all three directions is more likely to reveal weaknesses in the grid than refining only in one or two coordinate directions since the size of turbulent flow structures may be fixed by the grid resolution in a single direction. As grids were refined, the ability of DES to resolve more turbulent flow structures was clearly demonstrated.

References

[1] Spalart, P.R., Jou, W.H., Strelets, M. and Allmaras, S.R., 1997, "Comments on the Feasibility of LES for Wings, and on a Hybrid RANS/LES Approach,", *First AFOSR Int. Conf. on DNS/LES.*

[2] Strelets, M., 2001, "Detached Eddy Simulation of Massively Separated Flows", *AIAA Paper 01-0879.*

[3] Squires, K.D., Forsythe, J.R., Morton, S.A., Strang, W.Z., Wurtzler, K.E., Tomaro, R.F., Grismer, M.J. and Spalart, P.R., "Progress on Detached-Eddy Simulation of Massively Separated Flows", *AIAA 2002-1021*, January 2002.

[4] Spalart, P.R., 2001, "Young-Person's Guide to Detached-Eddy Simulation Grids," *NASA CR 2001-211032.*

[5] Strang, W.Z., Tomaro, R.F, Grismer, M.J., 1999, "The Defining Methods of Cobalt$_{60}$: a Parallel, Implicit, Unstructured Euler/Navier-Stokes Flow Solver," *AIAA 99-0786*, January 1999.

[6] Spalart, P.R. and Allmaras, S.R., 1994, "A One-Equation Turbulence Model for Aerodynamic Flows," *La Recherche Aerospatiale* **1**, pp. 5-21.

[7] Spalart, P.R. (2000), "Strategies for Turbulence Modeling and Simulations", *International Journal of Heat and Fluid Flow*, **21**, p. 252-263.

[8] Shur, M., Spalart, P. R., Strelets, M., and Travin, A, 1999, "Detached-Eddy Simulation of an Airfoil at High Angle of Attack", 4th Int. Symp. Eng. Turb. Modelling and Measurements, Corsica, May 24-26, 1999.

[9] Pirzadeh, S., 1996, "Three-dimensional Unstructured Viscous Grids by the Advancing Layers Method," *AIAA Journal*, **34**, pp. 43-49.

[10] Polhamus, E.C., Geller, E.W. and Grunwald, K.J., 1959, "Pressure and Force Characteristics of Noncircular Cylinders as Affected by Reynolds Number with a Method Included for Determining the Potential Flow about Arbitrary Shapes", *NASA TR R-46*.

[11] Squires, K.D., Forsythe, J.R. Spalart, P.R., 2001, "Detached-Eddy Simulation of the separated flow around a forebody cross-section", *Direct and Large-Eddy Simulation IV*, ERCOFTAC Series – Volume 8, B.J. Geurts, R. Friedrich and O. Metais, editors, Kluwer Academic Press, pp. 481-500.

[12] Steinbrenner, J., Wyman, N. and Chawner, J., 2000, "Development and Implementation of Gridgen's Hyperbolic PDE and Extrusion Methods", *AIAA 00-0679*, January 2000.

[13] Morton, S.A., Forsythe, J.R., Mitchell, A.M., Hajek, D., "DES and RANS Simulations of Delta Wing Vortical Flows", *AIAA 2002-0587*.

[14] Mitchell, A.M., Molton, P., Barberis, D., Delery, J., "Oscillation of Vortex Breakdown Location and Control of the Time-Averaged Location by Blowing," *AIAA Journal*, V. 38, No. 5, May 2000, pp. 793-803.

[15] Forsythe, J.R., Squires, K.D., Wurtzler, K.E. and Spalart, P.R., 2002, "Detached-Eddy Simulation of Fighter Aircraft at High Alpha", *AIAA 2002-0591*.

[16] Peters, G. and Walck, K., "Excerpts from the F-15E Stability and Control Database", *Personal Communication*, Dec. 2000.